

## Combined 3D-QSAR and Molecular Docking Analysis of Styrylquinoline Derivatives as Potent anti-cancer Agents

R. Kasmi<sup>a,\*</sup>, M. Bouachrine<sup>b,c</sup> and A. Ouammou<sup>a</sup>

<sup>a</sup>Faculty of Science, Dhar El Mahraz, Sidi Mohamed Ben Abdellah University, Fez, Morocco

<sup>b</sup>MCNS Laboratory, Faculty of Science, University Moulay Ismail, Meknes, Morocco

<sup>c</sup>EST Khenifra, Sultan Moulay Sliman University, Morocco

(Received 10 September 2021, Accepted 1 December 2021)

3D-QSAR has indeed established itself as a very useful component in the design of compounds with biological potential. The use of this tool will therefore make it possible to more easily target the modulations to be carried out in order to improve the inhibitory capacity of the series studied. Statistical analyses of CoMFA and CoMSIA molecular interaction field descriptors and the model validation methods they generate are presented and applied to the three-dimensional quantitative structure-activity relationships study of a series of 32 wild-types HCT116 p53 inhibitor styrylquinolines. The selected CoMFA and CoMSIA models were generated by the partial least squares "PLS" method and all had very good internal prediction and cross-validation coefficient values  $Q^2$  of 0.601 and 0.6, respectively. In view of the results obtained by the contour maps of the developed models as well as the results of molecular docking, new analogues of styrylquinoline were designed. The study of the physicochemical, pharmacokinetic, and potential toxicity properties shows that the two newly predicted compounds T1 and T3 presented a better ADMET profile, in particular a good gastrointestinal absorption, compared to the most active compound taken from the literature, which reveals their promising interest as potential new drug candidates against wild human colon cancer.

**Keywords:** CoMFA, CoMSIA, Molecular docking, HCT116 p53, Styrylquinoline, ADMET

### INTRODUCTION

In more than 50% of tumors, cancer cells have at least one mutated allele of the P53 gene. This suggests an involvement of this gene in cell carcinogenesis. The mutations are located throughout the coding sequence but the vast majority of them are located in the region of the sequence that codes for the DNA-binding protein domain [1].

During normal cell division, cases of DNA damage have been detected, which in most instances leads to DNA repair or apoptosis, which is enabled by the p53 protein [2]. In fact, under conditions of stress, the tumor suppressor protein plays a central role in the defense of cellular integrity. It can

act as a transcription factor by stimulating the expression of a large number of genes involved, among others, in apoptosis, cell cycle arrest due to G1 phase blockage or DNA repair, and thus protect the organism against the spread of potentially tumor precursor cells [3].

Mutations on both alleles of the p53 gene then lead to the abrogation of its functions and its absence at the nuclear level, which predisposes to the development of cancer. Due to its primordial activity for the cell, mutations in p53 provide a selective advantage to tumor cells, which explains its major role in the cancerization process. Thus several anti-cancer therapies, currently under study or already in clinical use for some, are proposed with the aim of reducing the volume of tumors or at least halting or slowing their progression [4]. A distinction in p53-targeted therapies [5] is made according to the expression by the tumor of the

\*Corresponding author. E-mail: [kasmi.rania1993@gmail.com](mailto:kasmi.rania1993@gmail.com)

mutated or wild-type form of p53: gene therapy and molecules restoring the functions of p53 for the first category, and molecules inhibiting the degradation of p53 for the second category.

Nowadays, the advancement of science relies mainly on several research activities. The interest shown in molecules containing heterocyclic rings results from the fact that these molecules constitute the basic skeleton, for a wide variety of compounds of chemical, biological, pharmacological and industrial interest. It is noted that two-thirds of the organic compounds, known in the literature, are heterocycles. They play an important role in most of the biochemical processes [6]. The demonstration of the very varied activities of the majority of these molecules encourages researchers to synthesize new series of heterocyclic products.

A study by Mrozek-Wilczkiewicz *et al.* [7] revealed that the most active styrylquinoline derivatives tested in the human colorectal carcinoma cell line HCT116 p53<sup>+/+</sup> and the glioblastoma cell line U-251, carrying the mutation can induce p53-independent apoptosis by blocking the cell cycle at the S-phase.

Quinoline is a heterocyclic aromatic organic compound. It has the formula C<sub>9</sub>H<sub>7</sub>N and was first obtained from coal tar in 1834 by Runge. Coal tar remains the main source of commercial quinoline. It boils at 238 °C and it is a colorless liquid with an odor resembling that of pyridine, and very hygroscopic. It is a tertiary base, which forms well-defined salts. Samples exposed to light for a long time turn yellow and later brown. It dissolves easily in hot water and common organic solvents.

The quinoline derivatives exhibit a very particular richness, all from the point of view of synthesis and reactivity of the quinoline derivatives. Due to the presence of several reactive sites quinolones are involved in alkylation, amination, sulfurization, condensation, and cycloaddition reactions. Studies carried out on these derivatives have shown that the structural modification improves its pharmacological profile, giving it a wide spectrum of biological activities[8].

Among the most important classes of heterocycles are the quinoline derivatives, which have shown a more favorable pharmacological profile, indeed these derivatives have wide applications in medicinal chemistry, including anti-inflammatory agents [9], antiasthmatics [10],

antibacterials [11], antifungals [12], antimicrobials [13], treatment of malaria [14], cardiovascular diseases [15], and what interests us, in particular, is the anti-tumor [16] application.

Styrylquinoline is a class of bioactive molecules with a quinoline nucleus that indicates therapeutic efficacy. For quinolines to have anti-tumor activity, they must be substituted in the C-8 position by the hydroxy or acyloxy group in order to chelate metal ions, as well as a substitution in the phenyl ring of the styryl group by an electron-withdrawing group, further increases the anti-cancer activity.

8-Hydroxyquinoline is an organic compound of formula C<sub>9</sub>H<sub>7</sub>NO, derived from heterocyclic quinoline hydroxylated on carbon 8, known for its chelating power with the ferrous ion (Fe<sup>2+</sup>) [17] necessary for the enzymatic catalysis of DNA biosynthesis, the name "oxines" is very practical, in particular for the description of complex-generating compounds, which can be called oxinates [18]. The fundamental property of styrylquinolines due to their flat aromatic structure is their ability to intercalate between the nucleic base pairs of the DNA [19], they bind covalently and/or pile up (stacking interaction) between two nitrogenous base plates within the double helix.

This intercalation can alter the topology of the DNA and modify or interrupt enzymatic processes such as replication. In addition, the intercalation of the most promising styrylquinolines may also cause the generation of excess reactive molecular oxygen species (ROS) [20], which subsequently contributes to oxidative stress induced by the imbalance in the prooxidant/antioxidant scale leads to oxidative damage in DNA and eventually causes p53-independent cell death, which may be a future strategy to restore the function of the tumor suppressor gene in the case of this mutation or deletion.

Our objective in this study is to establish a quantitative 3D model of structure-activity relationships of the wild-type inhibition of HCT116 p53<sup>-/-</sup> (exhibiting a p53 deletion) by a series of styrylquinolines using CoMFA and CoMSIA techniques [21], they are based on descriptors of three-dimensional structures, which resolves some of the major shortcomings inherent in conventional 2D techniques, which inherently neglect a large amount of stereochemical information. These approaches have been used to correlate

the biological activity of the reference set of active compounds with the spatial arrangement of many properties of the molecule such as steric, lipophilic, and electronic properties. These techniques can yield very high-quality models and have therefore been rapidly and widely used.

In an effort to assist in the development of novel anti-cancer agents belonging to the same styrylquinoline family, the use of the docking method [22] allows the prediction of the capacity or not of a molecule to bind to the active site of a protein based on the prediction of the conformation and orientation of that molecule upon binding to the receptor.

## MATERIALS AND METHODS

### Experimental Data

For this study, we have chosen to work on 40 molecules of styrylquinolines (Vinyl-quinoline) with R<sub>1</sub> and R<sub>2</sub> substituents as shown in Table 1, whose biological activity data were taken from the work of Mrozek-Wilczkiewicz *et al.* [7]. The bioassay test evaluates the effect of these compounds on wild human colon cancer cells (HCT116 lineage p53<sup>-/-</sup>) where inhibitory activity is reported in terms of IC<sub>50</sub>, we have expressed them in pIC<sub>50</sub> values as collected in Table 1 in the form of [-log<sub>10</sub>(IC<sub>50</sub> × 10<sup>-6</sup>)] to obtain the linear relationship with the independent variables [23].

The set of molecules is arbitrarily divided into two subsets: one of 8 molecules (about 20%) randomly selected, to evaluate the predictive power of the proposed models. The remaining 32 molecules (about 80%) constitute the learning set used in the construction of the 3D-QSAR models (CoMFA and CoMSIA) to establish the relationship between the structure and activity of this class of compounds.

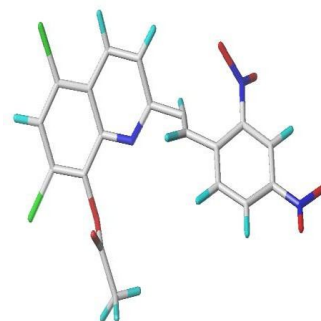
### Conformation and Alignment

First of all, the molecules were built using Chemdraw Professional 16.0, a preliminary minimization was carried out using Chem3D 16.0 *via* the MM2 molecular mechanics integrated into the software. Subsequently, the 40 molecules underwent a second optimization of their geometry thanks to the molecular modeling software (SYBYL-X2.0) "installed in a Windows 10 operating system on a PC equipped with an Intel Core i7 processor", by the Powell

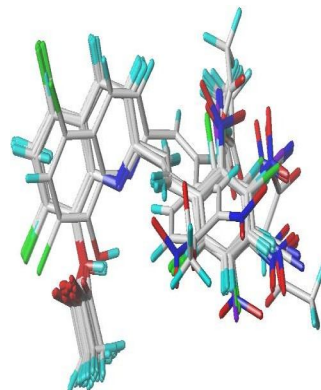
method (Force field: Tripos, atomic charges: Gasteiger-Hückel, dielectric constant: 1.0, Cutoff: 8 Å) [24]. The minimization was effected up to an energy gradient of 0.05 Kcal/(mol × Å).

The QSAR-3D type CoMFA or CoMSIA requires the prior alignment of structures in a particular conformation: the one adopted by each compound when it forms an active complex with the target. If there is no reference crystallographic data, no results of docking calculations, or a very rigid series, then the alignment of the active conformers is very difficult.

Manual alignment of this family of styrylquinolines is aligned on the reference structure 24c. It belongs more precisely to the dichloro derivatives, substituted in position 8 by an acyloxy and having 2,4-NO<sub>2</sub> in the phenyl ring, which makes it the most active of the series (Fig. 1). The superpositions between the different conformations were carried out according to SYBYL's simplealignment method [25]. The result of the superposition of the 40 molecules of the model is presented in Fig. 2.

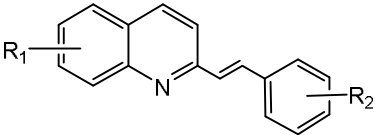


**Fig. 1.** Structure of the basic molecule 24c.



**Fig. 2.** Superpositions of the 40 compounds used for 3D-QSAR.

**Table 1.** Structure and Activity of the Studied Compounds for the Training and Test Set (\*)

Group			<i>p</i> IC <sub>50</sub>
	R <sub>1</sub>	R <sub>2</sub>	HCT116 (p53 <sup>-/-</sup> )
8a	8-OH	3-OAc	5.317
10a	8-OH	2-Cl	5.053
12a	8-OH	2,3-Cl	5.028
14a	8-OH	2-NO <sub>2</sub>	5.343
9b	8-OH	2-NO <sub>2</sub>	5.583
1c	5,7-Cl-8-OAc	2-OAc	5.057
3c	5,7-Cl-8-OAc	2-OAc-3,5-Cl	5.326
4c	5,7-Cl-8-OAc	2-OAc-3-Br-5-Cl	5.358
5c	5,7-Cl-8-OAc	2-OAc-3,5-I	5.409
6c	5,7-Cl-8-OAc	2-I	5.620
7c*	5,7-Cl-8-OAc	2-Cl	5.886
8c	5,7-Cl-8-OAc	2,6-Cl	5.218
9c*	5,7-Cl-8-OAc	2-Cl-6-F	5.564
10c	5,7-Cl-8-OAc	2-Br-6-F	5.538
11c	5,7-Cl-8-OAc	2,5-F	5.350
12c	5,7-Cl-8-OAc	2,6-F	5.348
13c*	5,7-Cl-8-OAc	2,6-F-3-Cl	5.317
15c	5,7-Cl-8-OAc	2-CN	6.119
16c	5,7-Cl-8-OAc	3-CN	5.833
17c*	5,7-Cl-8-OAc	4-CN	5.717
18c	5,7-Cl-8-OAc	2-OAc-3-NO <sub>2</sub>	5.583
19c*	5,7-Cl-8-OAc	2-OAc-5-NO <sub>2</sub>	5.444
20c	5,7-Cl-8-OAc	3-NO <sub>2</sub> -4-OAc	5.345
21c	5,7-Cl-8-OAc	2-NO <sub>2</sub>	6.108
22c	5,7-Cl-8-OAc	3-NO <sub>2</sub>	5.996
23c	5,7-Cl-8-OAc	4-NO <sub>2</sub>	5.697
24c	5,7-Cl-8-OAc	2,4-NO <sub>2</sub>	6.569
2d	5,7-Cl-8-OH	2-OAc-3,5-Cl	5.395
3d*	5,7-Cl-8-OH	2-OH-3-Br-5-Cl	5.588
4d	5,7-Cl-8-OH	2-Cl	5.544
5d	5,7-Cl-8-OH	2,3-Cl	5.398
6d	5,7-Cl-8-OH	2-Cl-6-F	5.347
8d	5,7-Cl-8-OH	2-CN	6.237
9d*	5,7-Cl-8-OH	3-CN	5.277
10d*	5,7-Cl-8-OH	4-CN	5.609
11d	5,7-Cl-8-OH	3-NO <sub>2</sub> -4-OAc	5.484
12d	5,7-Cl-8-OH	2-NO <sub>2</sub>	6.268
13d	5,7-Cl-8-OH	3-NO <sub>2</sub>	5.987
14d	5,7-Cl-8-OH	4-NO <sub>2</sub>	5.470
15d	5,7-Cl-8-OH	2,4-NO <sub>2</sub>	6.119

### The CoMFA and CoMSIA Descriptors

Certain techniques are used to develop models for the virtual screening of molecules, including CoMFA and CoMSIA. They thus make it possible to virtually create the active site of the therapeutic target by generating models from SAR results known from the literature.

For CoMFA as for CoMSIA, molecular interaction fields are calculated by the evaluation of the interaction potential between a probe and the molecule under study. The 3D descriptors require prior conformational alignment of all molecules used in the model. The CoMFA (Comparative Molecular Field Analysis) descriptors predict for a given conformer the electrostatic fields calculated according to the Lennard-Jones potential and the steric molecular fields according to the Coulomb potential that surround aligned molecules [26]. The fields are measured at each position of the probe, using principles of molecular mechanics. We generally take the carbon  $sp^3$  charged +1 or -1 as an atomic probe, which is placed at each mesh of a grid centered on the molecule (generally with a pitch of 1 or 2 Å) depends or not on the dielectric constant, with the application of an energy cutoff of 30 kcal mol<sup>-1</sup> [27].

The CoMSIA (Comparative Molecular Similarity Indices Analysis) descriptors tend to improve CoMFAs because they aim to compensate for too abrupt changes in energy potentials, which may be induced by the step between each mesh of the grid. The CoMSIA method [28] calculates 5 molecular fields related to 5 physico-chemical properties namely steric field, electrostatic, hydrophobic, hydrogen bond donor, and hydrogen bond acceptor, according to the Gaussian dependent method and no singularity is made depending on the atomic position, which allows a less pronounced change in the used properties. The default attenuation factor is 0.3 for all selected molecular fields. The Gaussian function is a good approximation of the Lennard-Jones and Coulomb potentials making the energy cut-off less pronounced and thus no energy threshold is necessary, which makes the CoMSIA models richer and easier to interpret.

### Partial Least Square Statistical Analysis (PLS)

The technique of partial least squares makes it possible to replace the initial space of the explanatory variables with a small dimensional space constituted from the linear

combinations of the initial explanatory variables, called "latent variables", which are orthogonal and constructed one after the other in an iterative way [29].

PLS statistical analysis through cross-validation [30] is the most commonly used method for correlating the biological activity values predicted by the model with the experimental biological activity values. Cross-validation is particularly useful in PLS because it also makes it possible to establish the number of components that optimizes the signal/noise ratio, it is common to perform a cross-validation of the Leave-one-out (LOO) type, which is implemented in SYBYL: a single compound is forgotten before each derivation and its activity is calculated by the corresponding model, it makes it possible to obtain the correlation coefficient  $Q^2$ , which expresses the internal forecasting power of the model.

A second model is then derived, without cross-validation but with the optimal number of components  $N$  indicated by the previous analysis. We obtain the correlation index  $R^2$ , the standard error of estimation, and the value  $F$  with the degrees of freedom of the model and the residual. The relative weight of each descriptor used in the model is also given to each analysis. High values for the  $R^2$  and  $Q^2$  indices are therefore necessary but are still insufficient to validate the quality of the model. The perfect validity is examined by external validation, which evaluates the generalization of the model, by the evaluation of a test set of 8 compounds, not used to build the model with obtaining the correlation index that describes the external forecasting power:  $R^2_{test}$ .

### Randomization Test

The most commonly used approach to check the robustness of a model is the randomization test of responses [31], this test asserts that the chance correlation plays no role during the development of the model. The values of the target variable ( $pIC_{50}$ ) are randomly redistributed over the whole training set and a new model is derived. the operation is repeated several times, the  $R^2$  and  $Q^2$  are supposed to be much lower than those of the initial model. Indeed, obtaining equivalent or even higher parameters would be a sign of an overlearning of the model, so it can be concluded that no acceptable QSAR model can be obtained by this statistical method on this data set.

## Molecular Docking

Molecular docking is a very useful process that aims to predict the probable interactions between ligands (substrate, activator, or inhibitor) and the amino acids making up the receptor (protein) structure in order to accelerate the search and discovery of new drugs *in silico* [32].

By consulting the PDB bank, the file of the receptor has been downloaded, it is a 3D protein structure whose code is 2GEQ, in the pdb format, obtained by X-ray diffraction and defined with a resolution of 2.3 Å. Since the complex is presented with two chains (Fig. 3), then one of the two is eliminated with the water molecules in order to speed up and simplify the calculations.

The inhibitors used in our work are designed with ChemDraw Professional and optimization of the geometry in SYBYL-X2.0 becomes necessary by the Powell method, using the: Tripos force field [33]. The minimization was performed up to an energy gradient of 0.05 kcal/(mol × Å) [34]. The molecules thus obtained are registered in pdb format. Once the pdb files are downloaded, the AutoDockTools-1.5.6 software [35] prepares the protein and ligand input files whose extension is pdbqt (AutoDock's own format), which contains the atoms and partial charges. The 2GEQ receptor is immersed in a three-dimensional grid largely encompassing the active site of the studied ligands and allowing the free rotation of the ligand in this site. All of these instructions are saved in a parameterization text file with the extension gpf (Grid Parameter File), the instructions contained in the gpf file are executed thanks to the AutoGrid sub-program, this involves calculating the affinity between the different types of atoms of the protein and the ligand.

The AutoDock program searches for docking solutions according to the parameters transmitted to it *via* dpf file (Dock parameters File), using the genetic algorithm to optimize the orientation of the ligands within the active sites. Docking results are generated in a text file with the extension dlj (Dock LOG). This file provides results by grouping the solutions into classes (clusters) according to their spatial proximity. The different conformations are classified by energy with the best solution being the one with the lowest value.

## Prediction of ADMET Properties

Besides an affinity that confers biological activity, a

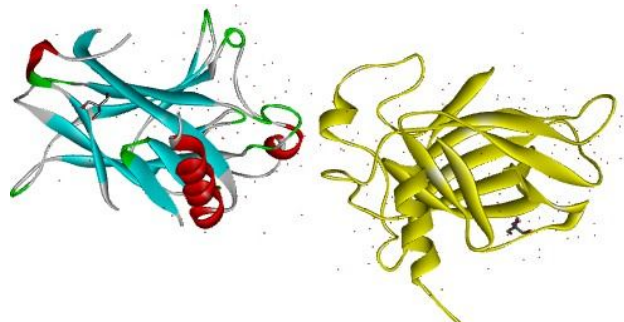


**Fig. 3.** The two A, B chains of the unsimplified protein (2GEQ).

potent molecule must reach its target in the body in sufficient concentration and remain there in a bioactive form long enough for the expected biological events to occur. Once a drug enters the body, it encounters a series of various obstacles on its way to the target. Overall, the properties of a drug with respect to its absorption, distribution, metabolism, excretion, and toxicity are often referred to as ADMET properties [36,37]. In our work, the SwissADME server available at (<http://www.swissadme.ch>) was used to predict the physicochemical properties and pharmacokinetics governing the ADME criteria of newly developed compounds and the most active inhibitor in the data set (24 C). Among these criteria, Lipinski's rule, Veber's rule, inhibition of cytochromes P450, gastrointestinal absorption, passage through the blood-brain barrier, accessibility to chemical synthesis, are determined.

## RESULTS AND DISCUSSION

### CoMFA Results

In order to generate the CoMFA model, 32 styrylquinolines are aligned and then superimposed on the most active 24c conformation as a template. The best model was obtained using steric and electrostatic fields with cutoffs of 30.0 kcal mol<sup>-1</sup>. The Leave-one-out analysis gives a cross-validated Q<sup>2</sup> coefficient value of 0.601 with six components N, and since this is greater than 0.5 it is a favorable indicator of the predictive power of the model. The non-cross-validated PLS analysis gives a conventional R<sup>2</sup> value of 0.961 and a standard error of estimate (SEE) of 0.084, this analysis gave an F (6;25) value of 103.79, as

**Table 2.** Statistics of the CoMSIA and CoMFA Models on all Training/Test Sets

Model	Q <sup>2</sup>	R <sup>2</sup>	SEE	F	N	R <sup>2</sup> <sub>test</sub>	Fractions				
							Ster	Elec	Hyd	Doc	Acc
CoMFA	0.601	0.961	0.084	103.79	6	0.704	0.336	0.664	-	-	-
CoMSIA	0.6	0.9	0.128	83.967	3	0.826	-	0.404	0.227	-	0.369

shown in Table 2.

A series of external tests of 8 styrylquinoline derivatives have been used to determine the accuracy of the model and the value of  $R^2_{test} = 70.4\%$  informs us about the validity of the model and its ability to predict values that were not used to generate it. The meaning of each descriptor and its contribution to the explanation of the biological activity was then verified, the electrostatic field has the greatest effect on the predictive power of the inhibitory activity of HCT116 p53<sup>-/-</sup> with a value of 66.4%, while the steric field is involved at 33.6% in the CoMFA model. Therefore the regions rich or poor in electrons is a key criterion for stimulating the anticancer activity of these compounds.

### CoMSIA Results

The 3D-QSAR model was realized by a PLS analysis of CoMSIA-type descriptors. The descriptors used are steric (S), electrostatic (E), hydrophobic (H), donor (D), and hydrogen bond acceptor (A) interaction fields. 31 possible combinations of these 5 descriptors were studied and the best model was obtained by combining three fields (electrostatic, hydrophobic, and hydrogen bond acceptor) of substituents of 32 molecules in order to evaluate their effects on anticancer activity. This "E, H, A" model uses an optimal number of 3 components with an internal predictive power  $Q^2$  of 0.6 established by the cross-validation test in the "leave-one-out" procedure (LOO). The model obtained is thus described by an internal correlation coefficient  $R^2$  of 0.9, a standard error of estimate (SEE) of 0.128 with an F value of 83.967, which is established by the no-validated PLS analysis.

However, the internal predictive power is not sufficient to evaluate the quality of the model, the combination of "E, H, A" descriptors gives us a better external predictive power, which is reported in Table 2 by a  $R^2_{test}$  coefficient of 0.826. The PLS also indicates the relative contribution of

each field in the model: Electrostatic field: 40.4%. Hydrophobic field: 22.7%. Acceptor field: 36.9%.

These percentages reveal that the contribution of the electrostatic field has the greatest impact on the inhibitory activity of the styrylquinoline derivatives studied against HCT116 p53<sup>-/-</sup> and therefore it is the majority field in the CoMSIA model.

### Interpretation of the Graphical Visualization of the Models

The main interest of CoMFA or CoMSIA models is that they allow building graphs for spatial visualization of structure-activity relationships. This gives direct and intuitive access to the model's explanations at the molecular scale. These graphs are based on the product of the variance of the points in a field by their coefficient in the model ( $StDev \times Coefficient$ ). They represent contour surfaces passing through points of the same value.

In order to make these contours comparable from field to field, the values are preliminarily transposed on a scale of 0 to 100. The contours are percentiles of the range of values present in the field. The user indicates to the software, which percentiles he wants to visualize. The levels 20% and 80% are generally used to represent respectively the regions of the field that are unfavorable and favorable to the activity, in this work, the 24c structure was adopted as a reference. These contour graphs show where changes in field explain variations in activity.

### CoMFA Contour Maps

In order to better understand the structure-activity relationships of our series of compounds, we will analyze the  $StDev \times Coefficient$  contour graphs. For the steric field, we have represented the 20% and 80% levels with different color codes, the green regions are favorable to hindrance and being occupied by large groups is desirable to increase

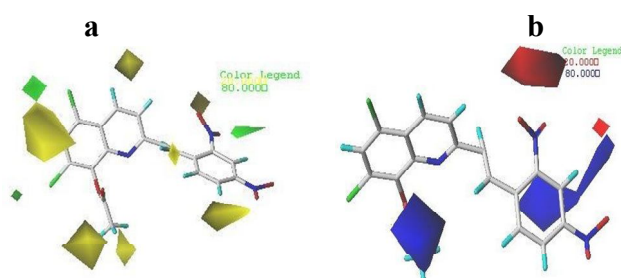


**Fig. 4.** (a) The steric field occupied by compound 24c. Regions are favorable to hindrance in green, unfavorable in yellow. (b) Compound 24c in the electrostatic field. Electronegative regions in red, electropositive regions in blue.

activity, while the yellow regions are unfavorable to hindrance, and must remain empty, otherwise, this will be reflected by a decrease in activity in the presence of the volume substituents at these contours, as shown in the Fig. 4a below. The electrostatic field is the richest in information, it is the one that contributes the most to explain the activity with a relative weight of 66.4%.

In Fig. 4b, the most active 24c compound in the series is represented with the zones where the variations in electronegativity have the most influence on the activity, the zones favorable to the increase in electronegativity are represented in red, those favorable to the decrease in electronegativity are in blue. We have two remarkable regions in this graph that can be easily interpreted, a clear unfavorable red contour in the model close to the nitro group at position 2 of the phenyl ring of the styryl group, reveals that a presence of electronegative groups in this area could exhibit good anti-tumor activity.

On the other hand, an important blue contour is located close to the acyloxy group in the C-8 position of the quinoline, indicating that this position must be positively charged and the existence of any electron-donating substituents is unfavorable if our purpose is to improve anticancer activity. If we take the two molecules 24c and 15d, they have the same basic structure, the same substituents except in the C-8 position, we can see that substitution of quinoline with a hydroxy group at the 15d molecule has led to a decrease in anti-tumor activity ( $pIC_{50} = 6.119$ ) compared with the most active one ( $pIC_{50} = 6.569$ ), which has an acyloxy group in the C-8

position.

### CoMSIA Contour Maps

There are certain similarities in the variation of electronegativity comparing the CoMSIA model to that of the CoMFA model, always with a dominance of the electrostatic field with a relative weight of 40.4%.

The only red contour is located near the NO<sub>2</sub> substituent at position 2 in the phenyl ring of the styryl group, it turns out that a substitution at this position affects the level of activity, since the presence of chlorine at this same position as shown by molecule 12a lowers the  $pIC_{50}$  value from 6.569 to 5.028, among other things the greater the effect of the electron donor group, the higher the antitumor activity. Ortho derivatives with cyano and nitro substituents showed the highest level of activity.

Two blue contour maps were found in our model, the first located at the C3 position in the phenyl ring of the styryl group, the second located at the C7 position of the quinoline, this indicates that it is preferable that these positions are depleted in electrons so that it carries electro-attracting substituents in order to increase the activity, the fact of finding the NO<sub>2</sub> and CN groups, which are the most electronegative located in the meta position of the analogues of the 24c molecule has lowered the activity value as in the 16C, 20C, and 22C compounds, as summarized in Figure 5a below.

The CoMSIA hydrophobic contour maps are illustrated in Fig. 5b. There are two yellow contours near the chloro substituents located at the C-5 and C-7 positions of the quinoline in compound 24c, it is a region, which promotes the presence of hydrophobic substituents if we want to increase anticancer activity.

If we examine compounds 8a, 10a, 12a, and 14a, we find that they are not substituted in the C-5 and C-7 positions of quinoline with the presence of the acyloxy group in the C-8 position, which makes  $pIC_{50}$  values lower than their chloroquine-based analogues. The replacement of the hydrogens in these positions by a methyl group increases the hydrophobicity, usually aromatic and aliphatic organic compounds are insoluble in water and improve the hydrophobicity, also the functional groups (electron donors or receptors) that can form a hydrogen bond with water can affect the hydrophobic behavior and subsequently an



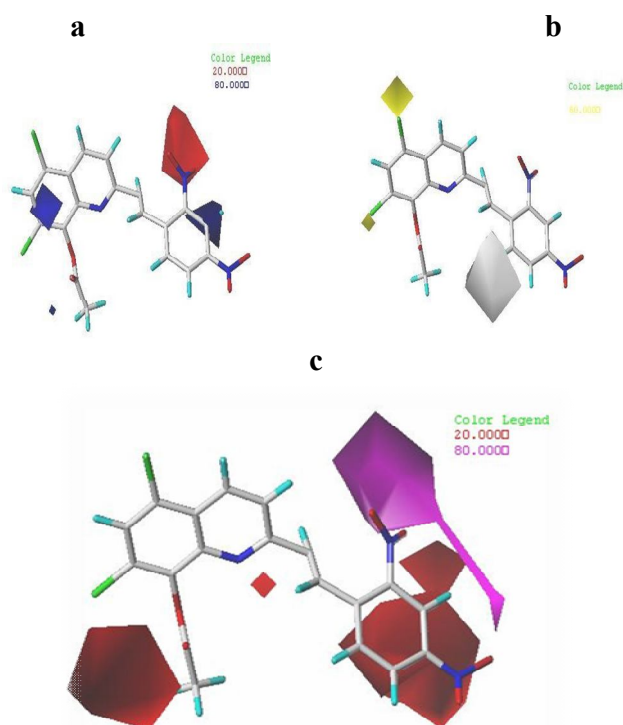


**Fig. 5.** (a) The StDev contour graph for the electrostatic field of the CoMSIA model, with a representation of the unfavorable regions by a red color, and the favorable regions by a blue color. (b) the hydrophobic field occupied by the most active compound 24c, the regions where the hydrophobic substituents are favorable are represented by a yellow color, the regions where the hydrophilic substituents are favorable are represented by graycolor. (c) The StDev contour graph for the hydrogen bond acceptor field of compound 24c; the zones where the hydrogen bond acceptor groups are significant are represented by magenta color; the zones where the hydrogen bond donor groups are significant are represented by red color.

increase in activity. The presence of a large gray contour around the C-6 position in the phenyl ring of the styryl group indicates that hydrophilic groups are beneficial in this region in order to enhance activity.

In Fig. 5c, the magenta contour near the C-2 position in the phenyl ring of the styryl group favors the hydrogen bond acceptor groups with the aim of improving the activity. This

is the reason why the compounds 24c ( $pIC_{50} = 6.569$ ) and 8d ( $pIC_{50} = 6.237$ ), whose substituents at the C2 position are nitro and cyano groups respectively, revealed the strongest inhibition, which is in concordance with the electrostatic contour map of this model, while the red contours expose the areas where hydrogen bond donating groups are significant.

### Overview of the Validation Tests

All the tests and statistical parameters of the CoMFA and CoMSIA models converge favorably.

The models are robust and have good  $Q^2$  coefficient values from the Leave-One-Out procedure. Although this technique allows the evaluation of the stability of the 3D-QSAR models with respect to the 32 molecules of the training set, but they do not allow in any case to demonstrate the predictive power of the models. The use of an external validation set: (7c\*, 9c\*, 13c\*, 17c\*, 19c\*, 3d\*, 9d\* and 10d\*), not employed for the development of the models, provided an excellent correlation between predicted and experimental activities (Table 3), with values of the  $R^2_{test}$  determination coefficient of 0.704 for the CoMFA model and 0.826 for the CoMSIA model. We, therefore, consider the models to be valid and we can use them to understand the structure-activity relationships of our styrylquinoline series and make activity forecasts for new structures.

### Y-randomization

In order to ensure that a 3D-QSAR model is reliable, y-randomization tests are one of the most widely used techniques, as it is not uncommon to obtain fortuitous correlations, namely a model with good statistical results ( $Q^2$ ,  $R^2$ ) for training, but involving descriptors that are unrelated to the activity being modeled. The randomization test allows us to affirm that the correlation of chance plays no role during the development of the models. The dependent variables are randomly disorganized, *i.e.* the  $pIC_{50}$  (obs) column has undergone several arbitrary mixtures, while the CoMFA and CoMSIA descriptors columns remain unchanged, new models are obtained, which must have very low performance.

The statistical parameters resulting from each reconstruction of the models are illustrated in Table 4,

**Table 3.** The  $pIC_{50}$  Activities Predicted and Experimental by the CoMFA and CoMSIA Models for the 32 Molecules of the Training Set and the 8 Test Molecules

N°	$pIC_{50}(\text{obs})$	$pIC_{50}(\text{pred})$				N°	$pIC_{50}(\text{obs})$	$pIC_{50}(\text{pred})$			
		CoMFA	Residu	CoMSIA	Residu			CoMFA	Residu	CoMSIA	Residu
10a	5.053	4.975	0.078	4.820	0.233	4c	5.358	5.426	-0.068	5.382	-0.024
10c	5.538	5.449	0.089	5.397	0.141	4d	5.544	5.478	0.066	5.581	-0.037
11c	5.350	5.281	0.069	5.435	-0.085	5c	5.409	5.376	0.033	5.399	0.01
11d	5.484	5.444	0.04	5.329	0.155	5d	5.398	5.492	-0.094	5.477	-0.079
12a	5.028	5.007	0.021	5.006	0.022	6c	5.620	5.675	-0.055	5.544	0.076
12c	5.348	5.413	-0.065	5.496	-0.148	6d	5.347	5.366	-0.019	5.505	-0.158
12d	6.268	6.123	0.145	6.063	0.205	8a	5.317	5.347	-0.03	5.298	0.019
13d	5.987	5.973	0.014	5.855	0.132	8c	5.218	5.321	-0.103	5.359	-0.141
14a	5.343	5.359	-0.016	5.394	-0.051	8d	6.237	6.217	0.02	6.254	-0.017
14d	5.470	5.469	0.001	5.615	-0.145	9b	5.583	5.585	-0.002	5.525	0.058
15c	5.967	6.113	-0.146	6.154	-0.187	10d*	5.609	5.704	-0.095	5.680	-0.071
.15d	6.119	6.292	-0.173	6.267	-0.148	13c*	5.317	5.779	-0.462	5.687	-0.37
16c	5.833	5.850	-0.017	5.886	-0.053	17c*	5.717	5.326	0.391	5.556	0.161
18c	5.583	5.575	0.008	5.562	0.021	19c*	5.444	5.677	-0.233	5.869	-0.425
1c	5.057	5.057	0	5.221	-0.164	3d*	5.588	5.602	-0.014	5.833	-0.245
20c	5.345	5.349	-0.004	5.350	-0.005	7c*	5.886	5.277	0.609	5.253	0.633
21c	6.108	6.08	0.028	5.999	0.109	9c*	5.564	5.463	0.101	5.505	0.059
22c	5.996	5.923	0.073	5.816	0.18	9d*	5.277	5.927	-0.65	5.922	-0.645
23c	5.697	5.572	0.125	8.638	-2.941						
24c	6.569	6.458	0.111	6.434	0.135						
2d	5.395	5.463	-0.068	5.455	-0.06						
3c	5.326	5.393	-0.067	5.380	-0.054						

which confirms that our models are more robust and are not due to hazard.

### Docking Studies

With a view to studying the anticancer mechanism in wild-type colon cells (HCT116) using this type of compounds, the molecular docking of these ligands is necessary to achieve rational results or even close to reality. This crucial study consists in seeking the most probable mode of ligand/receptor association, in other words respecting the experimental information available on this subject.

The molecular docking protocol adopted in this work consists in docking each ligand, considered flexible, in the active site of p53. The stopping parameters have been

pushed back to 2500.000 energy assessments and 27.000 generations. In order to have a statistically interesting sample of solutions, the genetic algorithm available in AutoDockTools-1.5.6 retained 50 conformations for each ligand, each docking experiment consisted of a series of 50 cycles, but what interests us more is the most stable conformation, *i.e.* the one with the lowest energy. As for the other simulation parameters, we have taken the program's default parameters.

In order to validate the credibility of the docking parameters, we compared the two TRS conformations considered as p53 inhibitors, that is to say, the one from the docking using these parameters and the experimental conformation from the 2GEQ complex. We present in Fig. 6 the superposition of redocked TRS and that of reference, the

**Table 4.**  $Q^2$ CV-Loo and  $R^2$  of the CoMFA and CoMSIA Models from the Randomization Test

Iteration	CoMFA		CoMSIA	
	$Q^2$	$R^2$	$Q^2$	$R^2$
1	-0.321	0.253	-0.29	0.5
2	-0.005	0.329	-0.028	0.287
3	-0.45	0.163	-0.393	0.166
4	-0.228	0.279	-0.207	0.264
5	-0.41	0.183	-0.434	0.186
6	-0.193	0.885	-0.096	0.431
7	-0.554	0.307	-0.485	0.320
8	-0.393	0.288	0.114	0.864
9	-0.145	0.334	-0.375	0.375
10	-0.573	0.266	-0.513	0.484
11	-0.485	0.229	0.403	0.776
12	-0.077	0.731	-0.666	0.331
13	-0.554	0.704	-0.631	0.296
14	-0.452	0.258	-0.222	0.464
15	-0.326	0.261	0.023	0.749
16	-0.420	0.708	-0.205	0.738
17	-0.583	0.488	-0.515	0.287
18	0.06	0.426	-0.401	0.333
19	-0.137	0.88	-0.397	0.284
20	-0.258	0.359	-0.3	0.66
21	0.031	0.495	-0.037	0.487
22	-0.224	0.410	-0.307	0.564
23	-0.194	0.236	-0.02	0.432
24	-0.008	0.528	-0.513	0.484
25	-0.51	0.383	0.144	0.62
26	-0.202	0.740	-0.214	0.773
27	-0.316	0.584	-0.34	0.282
28	0.076	0.703	0.100	0.76
29	-0.044	0.5	-0.522	0.276
30	0.117	0.836	0.142	0.70

figure shows that the two conformations superimpose well, which confirms the use of the parameters established in the continuation of our structural study.

The analysis of the results obtained by the docking simulations shows that the TRS ligand fits well into the active site of the p53 protein by means of 6 hydrogen

bonding interactions with 3 amino acids: ASP A:265, LEU A:108, and ASN A:128.

In order to clarify the mechanisms of interaction within the active site of the p53 receptor, the 2 most and least active molecules were chosen as references using the AutoDockTools-1.5.6 graphical interface. The results thus obtained were interpreted using Discovery Studio 2016 Client [38].

Figure 7 illustrates the binding mode of the most active compound 24c, it revealed the presence of two hydrogen bonds between the nitro group in the *para* position with the residues GLN A:97 and SER A:266. The phenyl ring of the

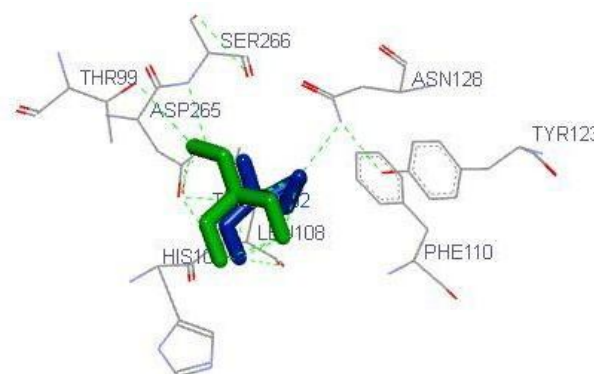


**Fig. 6.** Superposition of the two redocked and reference conformations of TRS in the active site of the protein.

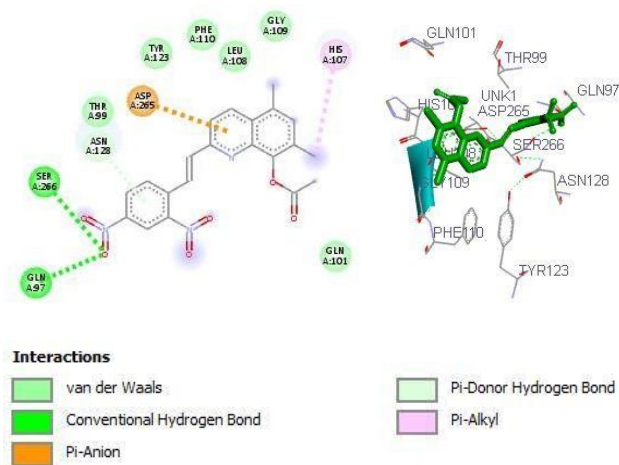


**Fig. 7.** The best positioning of compound 24c at the p53 binding site.

styryl group of the active compound 24c showed a Pi-donor hydrogen bond with the residue ASN A:128, which conforms with Fig. 5c where the red contours expose the zones in which the hydrogen bond donor groups are significant. Quinoline forms a non-covalent interaction from the Pi-anion with the amino acid ASP A:265, on the other hand, the chloro substituent at the C-7 position of quinoline appeared to constitute a Pi-Alkyl interaction of a hydrophobic nature, which is consistent with the yellow contours of the CoMSIA model that promotes the presence of hydrophobic substituents at this region.

The 2 interactions of the existing hydrogen bond type are the most primordial in terms of stabilization of the compound 24c inside the active site.

The benzene ring of the quinoline segment of the least active compound 12a forms an interaction by the Pi-sigma with the residue GLY A:109, the second is a hydrogen bond produced *via* the acetoxy group at the C-8 position with the same residue. While the pyridine ring of the quinoline segment exhibited a Pi-Lone Pair interaction with the amino acid LEU A:108, as depicted in Fig. 8. The two compounds 24c and 12a differ in the chemical nature of the substituents except for the OAc that is in common, this variation generates differences in terms of interaction with the residues of the active site, which leads to a decrease in the energies of the ligand/receptor complexes from  $E = -6.02 \text{ kcal mol}^{-1}$  for the most active molecule to  $E = -6.11 \text{ kcal mol}^{-1}$  for the least active molecule, which influences their affinity towards the biological target.

We can say that our study revealed the importance of some residues lining the active site, in particular GLN A:97, SER A:266, ASN A:128, ASP A:265, HIS A:107, GLY A:109, and LEU A:108 in the ligand bonds. They can be specifically targeted in order to design the structures of new, more powerful colon anti-cancer. This structural docking study constitutes a pathway in the development of new p53 inhibitors.

### Conception of New Active Compounds

We have constructed and validated a quantitative 3D model of the structure-activity relationships of a group of styrylquinolines inhibitors of HCT116 p53<sup>+</sup>, in the light of the results obtained by this model as well as by molecular docking simulation, we have been able to identify the nature

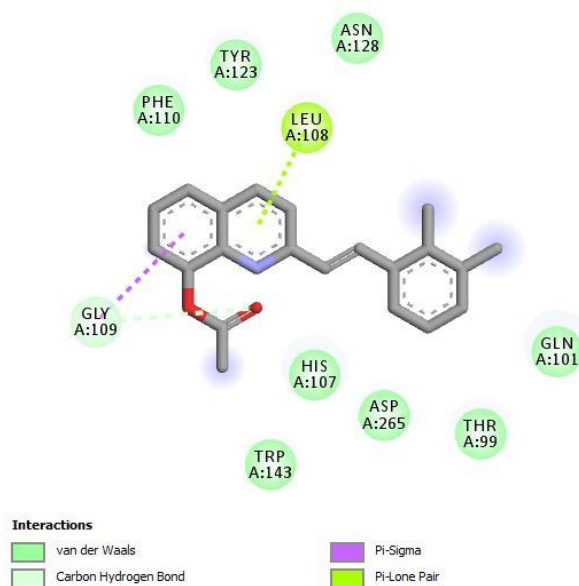


**Fig. 8.** The best positioning of compound 12a in the active site of p53, the bonds are shown in dotted lines.

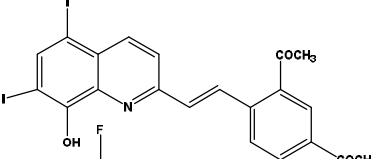
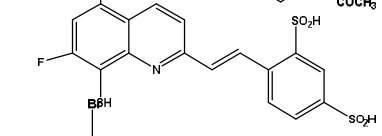
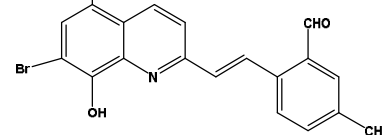
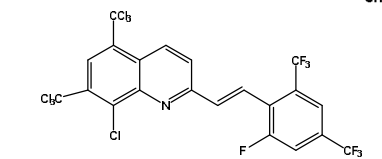
and position of groups that enhance activity. Four new structures (Table 5) have therefore been proposed accompanied by an activity prediction with more marked inhibitory values ( $pIC_{50} = 6,581$  by the CoMFA model;  $pIC_{50} = 6,901$  by the CoMSIA model) obtained by the compound T1.

Generally, there is a need to have a balance between hydrophobicity and hydrophilicity, so hydrophobicity is necessary for a molecule to be able to establish hydrophobic bonds with its target and can pass through the cell membrane, but certain hydrophilicity is mandatory for the therapeutic molecule to be soluble in the aqueous medium (blood, interstitial fluid, and cytoplasm) taking into account the parameters described by Lipinski (Table 5) does not in any way constitute an assurance of the bioavailability of the resulting molecule, but the integration of these rules associated with the choice of a privileged structure makes it possible to optimize the chances for a molecule to be bioavailable.

### Study of the Inhibitor-protein Interactions of Compound T1

Subsequently, in order to find out whether the results obtained by molecular docking are in agreement with those

**Table 5.** Proposal of Structures to Confirm and Enrich the Models

No	Structures	Predicted $pIC_{50}$		LogP	H-A	H-D	P.S	R.W	MW
		CoMFA	CoMSIA						
T1		6.581	6.901	5.84	4	1	66.73	4	583.164
T2		5.739	6.095	2.18	7	3	121.1	4	459.453
T3		6.411	6.603	5.05	4	1	66.73	4	461.109
T4		6.730	6.175	9.73	8	0	12.36	6	654.433

**Table 6.** The Scores of the 4 New Ligands Proposed as well as the Most Active Molecule 24c Following Molecular Docking with p53 Available under the PDB Code: 2GEQ

Inhibitors	$\Delta G$ Score AutoDock (kcal mol <sup>-1</sup> )	Conventional hydrogen bond Interaction	Hydrophobic interaction	Attractive charge interaction
T1	-7.06	LEU108, TYR123	His107, TRP143	
T2	-6.59	THR99, GLY109	TRP143, His107	
T3	-6.62	PRO125, GLN97, PHE110	LEU108, His107	ASP800
T4	-6.25	TYR123, ASN128, SER266	His107, TRP143	
24c*	-6.02	SER266, GLN97	His107	ASP265

of QSAR-3D, we carried out molecular docking on the 4 new molecules proposed by measuring their affinities using the AutoDockTools-1.5.6 programme. At the end of this test, it appears that these 4 compounds have lower binding energy than the starting compound 24c taken as a model on the basis of the literature [8], the results are summarised in Table 6 (in the supplementary material). We have limited ourselves to elucidating the interaction mechanisms involved between the p53 protein and the best-proposed

molecule T1 since it is characterised by inhibitory values ( $pIC_{50} = 6.581$  in the CoMFA model;  $pIC_{50} = 6.901$  in the CoMSIA model) better than that of the 24c compound, which was of the order of 6.458 and 6.434, respectively and whose interaction energy is clearly improved by a score of  $-7.06$  kcal mol<sup>-1</sup>.

The visual analysis allows us to see that the molecule is stabilised by several types of interactions and that this molecule has retained the same mode of binding as the 24c

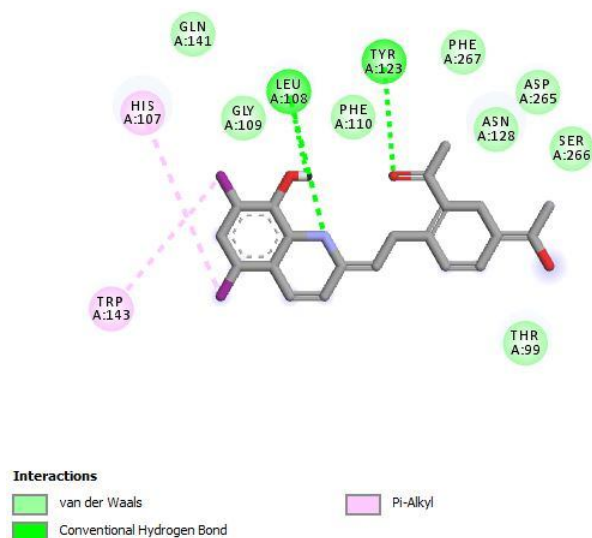


**Fig. 9.** Mode of interactions of the inhibitor T1 with the active site of 2GEQ.

molecule, but given the introduction of new substituents in positions 5, 7, and 8 of the quinoline as well as in the phenyl ring of the styryl group, this certainly keeps two hydrogen

bonds but with different amino acids, which are leucine 108 and tyrosine 123 represented in Fig. 9 (see in supplementary material).

The p53-compound T1 is also stabilised thanks to the hydrophobic interactions involving the residues His107 and TRP143.

### ADMET Properties

Several studies support the fact that a good drug candidate must possess, in addition to a high activity towards the target, ADMET properties compatible with a biological application. In this context, it was essential to reinforce our study by evaluating certain physicochemical and pharmacokinetic properties governing the ADMET criteria of the 4 new compounds by comparing their properties with those of the most active 24c molecule of the studied series.

**Physico-chemical properties.** Table 7 (in supplementary material) shows that the compounds T1 and T3, unlike the 24c molecule, comply perfectly with Lipinski's rule as well as that of Veber. These results indicate that both compounds can be used without posing

**Table 7.** The Relative ADME Profile of Candidate Compounds Obtained from the SwissADME Server

Properties	T1	T2	T3	T4	24c*
Formula	C <sub>21</sub> H <sub>15</sub> I <sub>2</sub> NO <sub>3</sub>	C <sub>17</sub> H <sub>11</sub> F <sub>2</sub> NO <sub>6</sub> S <sub>3</sub>	C <sub>19</sub> H <sub>11</sub> Br <sub>2</sub> NO <sub>3</sub>	C <sub>22</sub> H <sub>16</sub> F <sub>7</sub> N	C <sub>19</sub> H <sub>11</sub> Cl <sub>2</sub> N <sub>3</sub> O <sub>6</sub>
MW	583.16	459.46	461.10	427.36	448.21
(g mol <sup>-1</sup> )					
n.HA	4	9	4	8	7
n.HD	1	2	1	0	0
LogP	3.47	3.14	2.83	6.37	2.46
TPSA Å <sup>2</sup>	67.26 Å <sup>2</sup>	117.19 Å <sup>2</sup>	67.26 Å <sup>2</sup>	12.8 Å <sup>2</sup>	130.83 Å <sup>2</sup>
n.FL	4	4	4	4	6
Lipinski	Perfectly compliant	Perfectly compliant	Perfectly compliant	compliant	compliant
Veber	yes	no	yes	yes	Yes
Water solubility	Moderately soluble	Moderately soluble	Moderately soluble	Poorly soluble	Poorly soluble
Synthetic accessibility	3.00	3.15	2.65	3.06	3.15

MW = Molecular Weight; n.HA = number of Hydrogen Acceptors; n.HD = number of Hydrogen donor; n.FL = number of Flexible Link; LogP = water/octanol partition coefficient; TPSA = The topological polar surface.

problems of bioavailability by oral route. With an average solubility in water in contrast to that of the 24c molecule, which is poorly soluble, the T1 and T3 compounds can dissolve in aqueous media such as blood to reach their place of action in the organism with the desired concentration.

The last criterion studied concerns the accessibility to chemical synthesis. Remember that this criterion was evaluated in numbers ranging from 1 (easy to synthesize) to 10 (difficult to synthesize). In our case, the two scores 3.00 and 2.65 obtained with compounds T1 and T3 successively suggest that the chemical synthesis of the latter seems to be feasible on an experimental level.

**Pharmacokinetic properties.** A good drug candidate must be rapidly and completely absorbed from the gastrointestinal tract, distributed specifically to its site of action in the body, metabolized in a manner that does not impair body functions, and eliminated appropriately without causing harm [87]. In our work, we have predicted several pharmacokinetic properties of candidate compounds using the SwissADME server.

It emerges from Table 8 that the two compounds T1 and T3, unlike the 24c compound, exhibited a strong gastrointestinal absorption, which makes their access to the blood possible and this with an effective therapeutic concentration. However, these compounds as well as 24c present a low capacity to cross the blood-brain barrier. This criterion is much more important for compounds whose target is in the central nervous system, which is not the case here. Compounds T1 and T3 have been predicted to have an inhibitory effect against 2 of 5 cytochrome P450 isoforms.

Inhibition of these enzymes is an important source of undesirable drug interactions since changes in CYP enzyme activity can affect drug metabolism. Therefore, a potential inhibitory effect on CYP1A2, CYP2C19, CYP2C9, and CYP3A4 was observed in the case of compound 24c.

**Toxicity.** The PreADMET web server was used to evaluate the potential toxic effects of compounds T1 and T3. As shown in Table 9, both compounds T1 and T3 have been predicted to have mutagenic effects as well as carcinogenic potential towards rats. We also noted a moderate risk of inhibition of the hERG gene by these molecules. It should be remembered that inhibition of this gene causes disorders associated with cardiac rhythm. Moreover, the low values obtained for the acute toxicity of

**Table 8.** Pharmacokinetic Properties of Candidate Compounds as well as 24c

Properties	T1	T2	T3	T4	24c*
GI absorption	High	Lo w	High	Low	Low
BBB permeant	No	No	Yes	No	No
CYP1A2 inhibitor	No	Yes	No	No	Yes
CYP2C19 inhibitor	Yes	No	Yes	Yes	Yes
CYP2C9 inhibitor	Yes	No	Yes	No	Yes
CYP2D6 inhibitor	No	No	No	No	No
CYP3A4 inhibitor	No	No	No	No	Yes

GI: Gastro Intestinal; BBB: Blood-Brain Barrier; CYP: Cytochrome P450 family.

**Table 9.** The Relative Toxicity Profile of Candidate Compounds Obtained from the PreADMET Server

Parameter	T1	T3	24c*
Ames test	Mutagen	Mutagen	Mutagen
Carcinogenicity for mouse	Negative	Negative	Positive
Carcinogenicity for rat	Positive	Positive	Positive
hERG inhibition	Medium-risk	Medium-risk	Low-risk
Algae-at	0.0014975	0.00416775	0.00489284
Daphnia-at	0.00108204	0.00515239	0.0278552
Medakat-at	8.68453e-006	8.30315e-005	0.0018325
Minnow-at	3.50991e-005	0.000154987	7.85976e-005

these compounds on the 4 aquatic species are comparable to those obtained with the 24c molecule. This suggests that the acute toxicity of these compounds is relatively low.

In brief, the compounds T1 and T3, with a good ADME profile and a potentially high inhibitory power towards the target, can be proposed as novel inhibitors of HCT116 p53<sup>-/-</sup>. The information that we have provided regarding their potential toxicity will be very useful when optimizing them to become drug candidates.

## CONCLUSIONS

In order to generate new anticancer agents, the 3D-QSAR and molecular docking studies were employed to define the structural characteristics and the binding modes of styrylquinoline derivatives acting as inhibitors of HCT116 p53<sup>-/-</sup>. The statistical parameter values obtained by the CoMFA and CoMSIA/EHA models show that the latter is statistically significant with good predictive power, and this significance has been confirmed by the external validation methods, which proves that these models can be generalized on other structures different from styrylquinoline derivatives. Molecular docking simulation demonstrated how styrylquinoline analogues lodge in the active site of the p53 protein through their interactions with amino acids that play a crucial role in their anti-cancer activity. The results of the contour maps and the molecular docking analysis made it possible to highlight the compounds T1 and T3, which may be useful for the subsequent design of new inhibitors of HCT116 p53<sup>-/-</sup>. Furthermore, these molecules have shown promising results *in silico*, as well as an acceptable ADMET profile for biological application. This study would be of great use in optimizing the discovery of new drugs likely to treat cancer.

## ACKNOWLEDGEMENTS

We would like to express our gratitude to the Molecular Chemistry and Natural Substances Laboratory (MCNS), Department of Chemistry, Faculty of Science, Moulay Ismail University of Meknes, Morocco. We would also like to thank our dear Professor Mohammed Bouachrine, Director of the Higher School of Technology, Khenifra, Morocco for his outstanding support.

### Data Availability

The data that supports the findings of this study are available within the article.

## REFERENCES

- [1] Gudikote, J. P.; Cascone, T.; Poteete, A.; Sitthideatphaiboon, P.; Wu, Q.; Morikawa, N.; Zhang, F.; Peng, S.; Tong, P.; Li, L.; Shen, L.; Nilsson, M.; Jones, P.; Sulman, E. P.; Wang, J.; Bourdon, J. -C.; Johnson, F. M.; Heymach, J. V., Inhibition of nonsense-mediated decay rescues p53 $\beta/\gamma$  isoform expression and activates the p53 pathway in MDM2-overexpressing and select p53-mutant cancers, *J. Biological Chem.* **2021**, *297*, 101163. <https://doi.org/10.1016/j.jbc.2021.101163>.
- [2] Thayer, K. M.; Han, I. S. M., Chemical principles additive model aligns low consensus DNA targets of p53 tumor suppressor protein, *Comput. Biol. Chem.* **2017**, *68*, 186-193. <https://doi.org/10.1016/j.compbiolchem.2017.03.003>.
- [3] W. Dridi, R. Fetni, J. Lavoie, M.-F. Poupon, R. Drouin, The dominant-negative effect of p53 mutants and p21 induction in tetraploid G1 arrest depends on the type of p53 mutation and the nature of the stimulus, *Cancer Genetics and Cytogenetics.* **2003**, *143*, 39-49. [https://doi.org/10.1016/S0165-4608\(02\)00837-3](https://doi.org/10.1016/S0165-4608(02)00837-3).
- [4] Ramos, H.; Soares, M. I. L.; Silva, J.; Raimundo, L.; Calheiros, J.; Gomes, C.; Reis, F.; Monteiro, F. A.; Nunes, C.; Reis, S.; Bosco, B.; Piazza, S.; Domingues, L.; Chlapek, P.; Vleek, P.; Fabian, P.; Rajado, A. T.; Carvalho, A. T. P.; Veselska, R.; Inga, A.; Pinho e Melo, T. M. V. D.; Saraiva, L., A selective p53 activator and anticancer agent to improve colorectal cancer therapy, *Cell Reports.* **2021**, *35*, 108982. <https://doi.org/10.1016/j.celrep.2021.108982>.
- [5] Levine, A. J., Targeting therapies for the p53 protein in cancer treatments, *Annu. Rev. Cancer Biol.* **2019**, *3*, 21-34. <https://doi.org/10.1146/annurev-cancerbio-030518-055455>.
- [6] Rajesh, Y. B. R. D., Quinoline Heterocycles: Synthesis and Bioactivity, in: B. P. Nandeshwarappa, S. S. O. (Eds.), *Heterocycles-Synthesis and Biological Activities*, IntechOpen, **2020**. <https://doi.org/10.5772/intechopen.81239>.
- [7] Mrozek-Wilczkiewicz, A.; Kuczak, M.; Malarz, K.; Cieřlik, W.; Spaczyńska, E.; Musiol, R., The synthesis and anticancer activity of 2-styrylquinoline derivatives. A p53 independent mechanism of action, *Eur. J. Med. Chem.* **2019**, *177*, 338-349. <https://doi.org/10.1016/j.ejmech.2019.05.061>.
- [8] Lauria, A.; La Monica, G.; Bono, A.; Martorana, A., Quinoline anticancer agents active on DNA and DNA-



- interacting proteins: From classical to emerging therapeutic targets, *Eur. J. Med. Chem.* **2021**, *220*, 113555. <https://doi.org/10.1016/j.ejmech.2021.113555>.
- [9] Bekhit, A. A.; El-Sayed, O. A.; Aboulmagd, E.; Park, J. Y., Tetrazolo[1,5-a]quinoline as a potential promising new scaffold for the synthesis of novel anti-inflammatory and antibacterial agents, *Eur. J. Med. Chem.* **2004**, *39*, 249-255. <https://doi.org/10.1016/j.ejmech.2003.12.005>.
- [10] Afzal, O.; Kumar, S.; Haider, M. R.; Ali, M. R.; Kumar, R.; Jaggi, M.; Bawa, S., A review on anticancer potential of bioactive heterocycle quinoline, *Eur. J. Med. Chem.* **2015**, *97*, 871-910. <https://doi.org/10.1016/j.ejmech.2014.07.044>.
- [11] Chu, X. -M.; Wang, C.; Liu, W.; Liang, L. -L.; Gong, K. -K.; Zhao, C. -Y.; Sun, K. -L., Quinoline and quinolone dimers and their biological activities: An overview, *Eur. J. Med. Chem.* **2019**, *161*, 101-117. <https://doi.org/10.1016/j.ejmech.2018.10.035>.
- [12] Nakamoto, K.; Tsukada, I.; Tanaka, K.; Matsukura, M.; Haneda, T.; Inoue, S.; Murai, N.; Abe, S.; Ueda, N.; Miyazaki, M.; Watanabe, N.; Asada, M.; Yoshimatsu, K.; Hata, K., Synthesis and evaluation of novel antifungal agents-quinoline and pyridine amide derivatives, *Bioorg. Med. Chem. Lett.* **2010**, *20*, 4624-4626. <https://doi.org/10.1016/j.bmcl.2010.06.005>.
- [13] Teng, P.; Li, C.; Peng, Z.; Anne Marie, V.; Nimmagadda, A.; Su, M.; Li, Y.; Sun, X.; Cai, J., Facile accessible quinoline derivatives as potent antibacterial agents, *Bioorgan. Med. Chem.* **2018**, *26*, 3573-3579. <https://doi.org/10.1016/j.bmc.2018.05.031>.
- [14] van Schalkwyk, D. A.; Egan, T. J., Quinoline-resistance reversing agents for the malaria parasite Plasmodium falciparum, *Drug Resist. Update.* **2006**, *9*, 211-226. <https://doi.org/10.1016/j.drup.2006.09.002>.
- [15] Marella, A.; Tanwar, O. P.; Saha, R.; Ali, M. R.; Srivastava, S.; Akhter, M.; Shaquiquzzaman, M.; Alam, M. M., Quinoline: A versatile heterocyclic, *Saudi Pharmaceutical J.* **2013**, *21*, 1-12. <https://doi.org/10.1016/j.jsps.2012.03.002>.
- [16] Su, T.; Zhu, J.; Sun, R.; Zhang, H.; Huang, Q.; Zhang, X.; Du, R.; Qiu, L.; Cao, R., Design, synthesis and biological evaluation of new quinoline derivatives as potential antitumor agents, *Eur. J. Med. Chem.* **2019**, *178*, 154-167. <https://doi.org/10.1016/j.ejmech.2019.05.088>.
- [17] Prachayasittikul, V.; Prachayasittikul, V.; Prachayasittikul, S.; Ruchirawat, S., 8-Hydroxyquinolines: a review of their metal chelating properties and medicinal applications, *DDDT.* **2013**, *1157*. <https://doi.org/10.2147/DDDT.S49763>.
- [18] Feeney, R. E., The antagonistic activities of conalbumin and 8-hydroxyquinoline (oxine), *Arch. Biochem. Biophys.* **1951**, *34*, 196-208. [https://doi.org/10.1016/S0003-9861\(51\)80025-0](https://doi.org/10.1016/S0003-9861(51)80025-0).
- [19] Snyder, R. D., Assessment of atypical DNA intercalating agents in biological and in silico systems, *Mutation Research/Fundamental and Molecular Mechanisms of Mutagenesis.* **2007**, *623*, 72-82. <https://doi.org/10.1016/j.mrfmm.2007.03.006>.
- [20] Kim, S. J.; Kim, H. S.; Seo, Y. R. Understanding of ROS-inducing strategy in anticancer therapy, *Oxidative Medicine and Cellular Longevity.* **2019**, *2019*, 1-12. <https://doi.org/10.1155/2019/5381692>.
- [21] Zhi, H.; Zheng, J.; Chang, Y.; Li, Q.; Liao, G.; Wang, Q.; Sun, P., QSAR studies on triazole derivatives as sglt inhibitors via CoMFA and CoMSIA, *J. Mol. Struct.* **1098**, **2015**, 199-205. <https://doi.org/10.1016/j.molstruc.2015.06.004>.
- [22] Issa, N. T.; Badiavas, E. V.; Schürer, S., Research techniques made simple: Molecular docking in dermatology-A foray into *in silico* drug discovery, *J. Invest. Dermatol.* **2019**, *139*, 2400-2408.e1. <https://doi.org/10.1016/j.jid.2019.06.129>.
- [23] Kasmi, R.; Hadaji, E.; Chedadi, O.; El Aissouq, A.; Bouachrine, M.; Ouammou, A., 2D-QSAR and docking study of a series of coumarin derivatives as inhibitors of CDK (anticancer activity) with an application of the molecular docking method, *Heliyon.* **2020**, *6*, e04514. <https://doi.org/10.1016/j.heliyon.2020.e04514>.
- [24] Aparoy, P.; Suresh, G. K.; Kumar Reddy, K.; Reddanna, P., CoMFA and CoMSIA studies on 5-hydroxyindole-3-carboxylate derivatives as 5-lipoxygenase inhibitors: Generation of homology model and docking studies, *Bioorg. Med. Chem. Lett.* **2011**, *21*, 456-462. <https://doi.org/10.1016/j.bmcl.2010.10.119>.
- [25] Ghaleb, A.; Aouidate, A.; Ghamali, M.; Sbai, A.;

- Bouachrine, M.; Lakhlifi, T., 3D-QSAR modeling and molecular docking studies on a series of 2,5 disubstituted 1,3,4-oxadiazoles, *J. Mol. Struct.* **2017**, *1145*, 278-284. <https://doi.org/10.1016/j.molstruc.2017.05.065>.
- [26] Fasihi Mohd Aluwi, M. F.; Rullah, K.; Koeberle, A.; Werz, O.; Abdul Razak, N.S.; Wei, L.S.; Salim, F.; Ismail, N.H.; Jantan, I.; Wai, L. K., Design and synthesis of a novel mPGES-1 lead inhibitor guided by 3D-QSAR CoMFA, *J. Mol. Struct.* **2019**, *1196*, 844-850. <https://doi.org/10.1016/j.molstruc.2019.07.004>.
- [27] Bolden, S.; Boateng, C. A.; Zhu, X. Y.; Etukala, J. R.; Eyunni, S. K.; Jacob, M. R.; Khan, S. I.; Ablordeppey, S. Y., CoMFA studies and *in vitro* evaluation of some 3-substituted benzylthio quinolinium salts as anticryptococcal agents, *Bioorgan. Med. Chem.* **2013**, *21*, 7194-7201. <https://doi.org/10.1016/j.bmc.2013.08.043>.
- [28] Ganguly, S.; Mishra, R., Comparative molecular similarity indices analysis of 1-(naphthylalkyl)-1H-imidazole analogs with antiepileptic activity, *J. Young Pharmacists.* **2010**, *2*, 388-393. <https://doi.org/10.4103/0975-1483.71635>.
- [29] Li, H. -D.; Xu, Q. -S.; Liang, Y. -Z., libPLS: An integrated library for partial least squares regression and linear discriminant analysis, *Chemometr. Intell. Lab. Systems.* **2018**, *176*, 34-43. <https://doi.org/10.1016/j.chemolab.2018.03.003>.
- [30] Lavoie, F. B.; Langlet, A.; Muteki, K.; Gosselin, R., Likelihood maximization inverse regression: A novel non-linear multivariate model, *Chemometr. Intell. Lab. Systems.* **2019**, *194*, 103844. <https://doi.org/10.1016/j.chemolab.2019.103844>.
- [31] Lipiński, P. F. J.; Szurmak, P., SCRAMBLE'N'GAMBLE: a tool for fast and facile generation of random data for statistical evaluation of QSAR models, *Chem. Pap.* **2017**, *71*, 2217-2232. <https://doi.org/10.1007/s11696-017-0215-7>.
- [32] Kasmi, R.; Hadaji, E.; Bouachrine, M.; Ouammou, A., QSAR and molecular docking study of quinazoline derivatives as anticancer agents using molecular descriptors, *Materials Today: Proceedings.* **2020**, S221478532033844X. <https://doi.org/10.1016/j.matpr.2020.05.283>.
- [33] Clark, M.; Cramer, R. D.; Van Opdenbosch, N., Validation of the general purpose tripos 5.2 force field, *J. Comput. Chem.* **1989**, *10*, 982-1012. <https://doi.org/10.1002/jcc.540100804>.
- [34] Tsai, K. -C.; Chen, Y. -C.; Hsiao, N. -W.; Wang, C. -L.; Lin, C. -L.; Lee, Y. -C.; Li, M.; Wang, B., A comparison of different electrostatic potentials on prediction accuracy in CoMFA and CoMSIA studies, *Eur. J. Med. Chem.* **2010**, *45*, 1544-1551. <https://doi.org/10.1016/j.ejmech.2009.12.063>.
- [35] Morris, G. M.; Goodsell, D. S.; Halliday, R. S.; Huey, R.; Hart, W. E.; Belew, R. K.; Olson, A. J., Automated docking using a Lamarckian genetic algorithm and an empirical binding free energy function, *J. Comput. Chem.* **19** (n.d.) 24.
- [36] Hane, U.; Rahman, Md. R.; Matin, M., Synthesis, PASS, *in silico* ADMET and thermodynamic studies of some galactopyranoside esters, *PCR.* **2021**, *9*. <https://doi.org/10.22036/pcr.2021.282956.1911>.
- [37] Matin, M. M.; Islam, N.; SiDdiKa, A.; Bhattacharjee, S. C., Regioselective synthesis of some rhamnopyranoside esters for PASS prediction, and ADMET studies, *Journal of the Turkish Chemical Society Section A: Chemistry.* **2021**, *8*, 363-374. <https://doi.org/10.18596/jotcsa.829658>.
- [38] Discovery Studio Predictive Science Application| Dassault Systèmes BIOVIA, (n.d.). <https://www.3dsbiovia.com/products/collaborative-science/biovia-discovery-studio/>.